Eur. Phys. J. B **13**, 685–694 (2000)

THE EUROPEAN PHYSICAL JOURNAL B

EDP Sciences
© Società Italiana di Fisica
Springer-Verlag 2000

Superconductor order parameter symmetry in UPd_2Al_3

N. Bernhoeft[a]

DRFMC-LCP, Centre d'Études Nucléaires, CEA Grenoble, 38054 Grenoble Cedex 9, France

Received 16 July 1999

Abstract. The heavy fermion compound UPd_2Al_3 has attracted much interest on account of the coexistence of antiferromagnetism and superconductivity at temperatures below 2 K. The antiferromagnetic fluctuations provide, principally *via* inelastic neutron scattering, a window on the low frequency dynamics in this material. By an analysis of neutron scattering data, and taking into consideration results from other experimental probes, it is suggested which sheet(s) of the f-electron Fermi surface may play an active role in forming the superconducting state in UPd_2Al_3. The proposed scheme sheds new light on previously reported anomalies in this material.

PACS. 74.70.Tx Heavy-fermion superconductors – 78.70.Nx Neutron inelastic scattering

1 Introduction

The transition to the superconducting phase breaks the global gauge symmetry of the normal state. Additional symmetries may be broken at T_c yielding so called "unconventional" superconducting states [1]. Such novel phases are of great current interest as they may include examples of self correlated (self organised) electronic systems. Materials susceptible to unconventional pairing mechanisms may be expected to exhibit strong electronic correlations in the normal phase, favourable candidates to date include the heavy fermion, high temperature, and organic superconductors. In view of its primary significance, and since it may shed light upon the microscopic pairing mechanism, the identification of the symmetry of the superconducting order parameter in these materials has been the object of many studies. The superconducting energy gap, Δ, which arises in microscopic theories of the superconducting state, is expected to be proportional to, and to have the same symmetries as, the superconducting order parameter [2]. Studies of the energy gap are thus used to elucidate the nature of the order parameter. Techniques to probe the symmetry and magnitude of Δ include electron tunneling, thermal conductivity, infra red absorption and nuclear magnetic resonance. These probes have, unfortunately, limited spectral capacity; for example, whilst electron tunneling measures $|\Delta|$ with good energy resolution it relies on the barrier thickness and its uniformity to probe the spatial symmetry of Δ within the Brillouin zone; thermal conductivity relies on the sample geometry to give the heat flow directionality with respect to the crystalline axes; infra red absorption is limited in momentum transfer to $q \sim 0$ and nuclear resonance techniques, being local probes of the magnetisation, give Brillouin zone integrals measured at very low ($\omega \sim 0$ on the scale of Δ) energies. In some instances, inelastic neutron scattering may provide a tool capable of simultaneous energy and momentum resolution on the appropriate scales. We report on the use of this technique to gain unique information on the symmetry and magnitude of Δ and make a tentative identification of the sheet(s) of the Fermi surface active in the formation of the condensate in the heavy fermion superconductor UPd_2Al_3.

UPd_2Al_3, which crystallises in the hexagonal $PrNi_2Al_3$ structure (space group $P6/mmm$) with lattice constants $a = 5.350$ Å and $c = 4.185$ Å, has been subject of numerous investigations [3–8]. The compound appears to occupy a special place amongst the heavy fermion superconductors in that it exhibits a strong antiferromagnetic polarisation below $T_N = 14.3$ K, amounting to 0.85 μ_B per uranium ion at low temperatures, which *coexists* with a superconducting ground state below $T_c = 2$ K. In comparison, the other classic heavy fermion superconductors, UPt_3 and URu_2Si_2, pass into the superconducting phase from a possibly dynamical, rather than static long range ordered, antiferromagnetic state of very weak polarisation (~ 0.03 μ_B per uranium ion). The stable moment in UPd_2Al_3 is accompanied by an enhanced spectrum of low energy fluctuations around the antiferromagnetic propagation vector $\mathbf{Q}_0 = (0, 0, 0.5)$ making it an ideal candidate for an investigation of the superconducting order parameter as imaged through the magnetic fluctuation spectrum. The moments, which are principally associated with the f-electron polarisation of the uranium ions, are coupled ferromagnetically and lie in the basal plane [9–13]. The breaking of hexagonal symmetry by the antiferromagnetic moment is ignored in this article for notational convenience; it has, however, been taken into account in the calculations.

[a] e-mail: bern@drfmc.ceng.cea.fr

The analysis, in the superconducting phase, of the (antiferro)-magnetic excitations measured by high resolution, inelastic, neutron scattering sheds valuable light on the low frequency dynamics of the electronic quasiparticles. In particular, one is able to monitor changes in the amplitude and spectral form of the magnetic excitations on passing below T_c. The observed changes are significant [14–21]. The quasielastic scattering in the normal phase, which is strongly focused around the antiferromagnetic Bragg peaks at $\mathbf{Q}_0$ and which may be associated with transitions between electronic quasiparticle states, is replaced by an enhanced (by almost a factor of 2) inelastic peak in the low temperature superconducting state [19–21]. The spin wave contribution to the scattering cross section, which occurs for energy transfers greater than 1.3 meV ($\sim k_B T_N$), is not so dramatically affected by the superconducting phase transition.

Within a model framework of the antiferromagnetic superconducting phase, one may understand both the enhancement and change from quasielastic to inelastic nature of the low energy scattering as arising from processes in which the incoming neutron beam looses energy and momentum to the condensate and creates quasiparticle excitations. We illustrate, using a simple (even parity, singlet) pairing approximation, how the momentum and energy dependence of the scattering constrain the symmetry and magnitude of the gap function. The form factor of the scattering, which exhibits a slow fall off of intensity with momentum transfer [20], indicates that both the spin wave and the low energy features are associated with f-electron like orbitals of the Fermi surface. The anisotropy of the scattering, that is, its wave vector dependence around $\mathbf{Q}_0$, allows a tentative identification of the sheet(s) of the Fermi surface contributing to the observed response. Below T_c these sheets are, by inference, active in the formation of the condensate. The identified Fermi sheet(s), the symmetry of the gap function and its magnitude are compatible with estimates made, for momentum transfers parallel to the c^*-axis, by tunneling junction spectroscopy [22–24].

2 Data analysis

2.1 Analysis of neutron spectra

The analysis of the neutron spectra rests on two assumptions. First, that the major effect on passing below T_N is to introduce an antiferromagnetic potential which halves the dimension of the unit cell, in reciprocal space, along the c^* axis. Thereafter, as far as the low energy quasiparticle excitations are concerned the system looks paramagnetic in as much as there is assumed to be no energy splitting of the spin states.

The second assumption is that the observed magnetic scattering, all of which is associated with the f-electron response, and which may broadly be divided into two parts, represented in the normal phase as (i) a quasielastic and (ii) a (gapped) spin wave response, is best analysed as a whole. To make the analysis we consider the total susceptibility when the magnetisation of sub-system (i) is coupled in a mean field approximation with the magnetisation of sub-system (ii) [18–21,25–30]. The coupling constant is taken to be energy, momentum and temperature independent, *i.e.* the effect of the field due to sub-system (i) is instantaneous and local on the magnetism of sub-system (ii). This constraint may be relaxed in a more realistic model. On passing into the superconducting phase, since a rigorous theory of the magnetic excitation spectra in the antiferromagnetic-superconducting phase is not yet available, we assume that the similar coupling occurs between the quasiparticle excitations and the spin wave mode.

The presence of the antiferromagnetic moment suppresses time reversal invariance. Central to the analysis is the idea that degenerate energy levels may however exist under the combined operation of time reversal and translation by a lattice vector [31–33] which allows one to consider superconductor pairing based on the mutual attraction of degenerate quasiparticle states. Alternative choices of the pairing condition in the antiferromagnetic state have been raised in the literature [34–37]. In this respect we note that the consequences of the (simultaneous) occurrence of triplet pairing has neither been considered nor excluded by the analysis since the simple model is capable of reproducing the key features of the inelastic spectra. Thus, in the following analysis, the condensate involves the pairing $(\mathbf{k}\uparrow, -\mathbf{k}\downarrow)$ where $\mathbf{k}$ is a wave vector in the antiferromagnetic Brillouin zone.

2.2 The magnetic susceptibility

Following the mean field coupling scheme, the total susceptibility of sub-system (i) in combination with subsystem (ii) may be written:

$$\chi = \frac{\chi_1 + \chi_2 + 2\lambda\chi_1\chi_2}{1 - \lambda^2\chi_1\chi_2} \tag{1}$$

where χ_1 and χ_2 are the starting susceptibilities (*i.e.* with all interactions apart from the mean field coupling between χ_1 and χ_2 switched on) and λ represents the coupling coefficient between the low, χ_1, and intermediate, χ_2, frequency modes [18–21,25–30]. Such a mean field model acts as low frequency amplifier since, in this limit, the real part of χ tends to a constant whilst the imaginary part is proportional to the frequency [38]. This, for the dissipative component of the total susceptibility, as $\omega \to 0$, yields a denominator, $1 - \lambda^2 \mathrm{Re}[\chi_1]\mathrm{Re}[\chi_2]$, whilst at high frequencies the bare susceptibilities must vanish and the denominator goes to unity. Thus the low frequency response will be enhanced by a generalised Stoner factor. In the limit, $\chi_1 \ll 1/\lambda \ll \chi_2$, a simplification of equation (1) has been used previously to describe, for example, $f-d$ interactions in actinides [39]. In our case, where the conduction electrons which condense into the superfluid state have heavy quasiparticle f character (witness the jump in specific heat at T_c [3]) and we do not know, *a priori*, the relative magnitudes of the terms, it is more reasonable to keep the full expression. Keeping the full equation involves no extra parameters. In either case, it is the origin

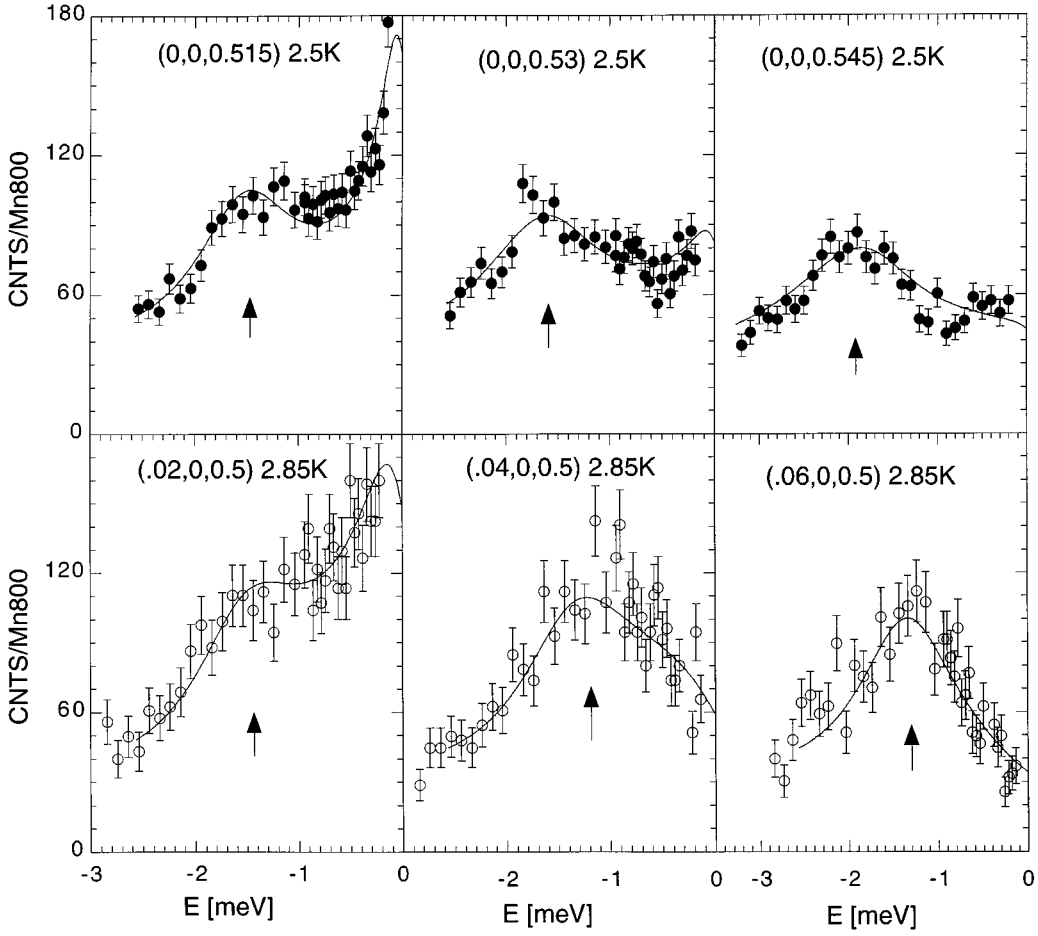

Fig. 1. The spin wave dispersion is plotted for small wave vectors $\mathbf{q}$ around $\mathbf{Q}_0$. The dispersion parallel to c^*, top three frames, is much stiffer than that parallel to a^*, bottom three frames. The stiffness constants are $D_{c^*} \sim 120 \pm 10$ meV Å^2 and $D_{a^*} \sim 20 \pm 10$ meV Å^2 respectively. The antiferromagnetic Bragg peak and the incoherent elastic scattering which fall within the elastic window of the spectrometer, ± 0.14 meV about $E = 0$, are not shown.

and structure of χ_1 as a function of temperature and wave vector which is of central interest.

The focus in this paper is on the form and interpretation of the low frequency component, χ_1, in the superconducting phase. If one accepts that the enhanced low frequency scattering, which appears uniquely in the superconducting phase, is driven by the condensate, general arguments (see under Eq. (2)) yield the symmetry of the gap function [19–21] at least for the dominant sheets of the Fermi surface probed by this technique. That this scattering may be related to the condensate is primarily supported by the experimental observations that it is suppressed on passing to the normal state either by increasing temperature or by an applied magnetic field greater than H_{c2} [14–21]. This conclusion is reinforced by the fall in the Knight shift below T_c [40] and the measured reduction of specific heat on passing to low temperatures [3,8]. The small residual specific heat at the lowest temperatures ($\gamma \sim 9$ mJmol^{-1}K^{-2} [8]) implies a paucity of quasiparticle excitations, and hence, a vanishing quasiparticle susceptibility. If there were no contribution from the condensate to χ_1 at the lowest temperatures one would observe $\chi \approx \chi_2$, the unrenormalised high frequency component of the susceptibility (*i.e.* the bare spin wave).

2.3 Spin wave spectra

Before passing to the low energy response below T_c we briefly consider the measured spin wave anisotropy in relation to the proposed Fermi surface. The calculated Fermi surface [41,42] has four principal sheets of predominately f-electron character. We use the descriptive notation of Knopfle *et al.* [41] who label, in their Figures 5 and 6, these sheets as, "cigar", "cylinder", "party hat", and "eggs". Where available we use de Haas-van Alphen (dHvA) data [41–43] to the estimate principal (average) Fermi surface radii and the effective masses to model the local dispersion of the quasiparticle bands. In an itinerant system one anticipates the spin wave dispersion to vary inversely with the effective mass [44]. As may be seen in Figure 1 the spin wave dispersion, $\hbar\omega(q) = \varepsilon_{\rm gap} + Dq^2$, with stiffness D, around $\mathbf{Q}_0$ is significantly steeper along c^* than along a^*. Looking at the Fermi surface the "cigar",

$$\chi(\mathbf{q},\omega) = \sum_{\mathbf{k}} \frac{1}{2}\left[1 + \frac{\xi(\mathbf{k}+\mathbf{q})\xi(\mathbf{k}) + \cos[\Phi(\mathbf{q})]|\Delta(\mathbf{k}+\mathbf{q})||\Delta(\mathbf{k})|}{E(\mathbf{k}+\mathbf{q})E(\mathbf{k})}\right]\frac{f(\mathbf{k}+\mathbf{q}) - f(\mathbf{k})}{\omega - [E(\mathbf{k}+\mathbf{q}) - E(\mathbf{k})] - \mathrm{i}\Gamma}$$
$$+ \sum_{\mathbf{k}} \frac{1}{4}\left[1 - \frac{\xi(\mathbf{k}+\mathbf{q})\xi(\mathbf{k}) + \cos[\Phi(\mathbf{q})]|\Delta(\mathbf{k}+\mathbf{q})||\Delta(\mathbf{k})|}{E(\mathbf{k}+\mathbf{q})E(\mathbf{k})}\right]\frac{1 - f(\mathbf{k}+\mathbf{q}) - f(\mathbf{k})}{\omega - [E(\mathbf{k}+\mathbf{q}) + E(\mathbf{k})] - \mathrm{i}\Gamma}$$
$$- \sum_{\mathbf{k}} \frac{1}{4}\left[1 - \frac{\xi(\mathbf{k}+\mathbf{q})\xi(\mathbf{k}) + \cos[\Phi(\mathbf{q})]|\Delta(\mathbf{k}+\mathbf{q})||\Delta(\mathbf{k})|}{E(\mathbf{k}+\mathbf{q})E(\mathbf{k})}\right]\frac{1 - f(\mathbf{k}+\mathbf{q}) - f(\mathbf{k})}{\omega + [E(\mathbf{k}+\mathbf{q}) + E(\mathbf{k})] - \mathrm{i}\Gamma}\,. \quad (2)$$

"cylinder" and "party hat" have anisotropy but in the opposite sense and so we are lead to propose that the "egg" shaped part of the Fermi surface plays a principal role in the spin wave response for small $\mathbf{q}$ about $\mathbf{Q}_0$[1].

2.4 Neutron spectra below T_c

We proceed in the calculation below T_c as follows; first we calculate the bare spin susceptibility above the superconducting ground state following equation (2), and then make an analytical approximation to the spectral form which is inserted into the second stage of the calculation where the mean field coupling, equation (1), is performed.

The spin susceptibility of the excited quasiparticles above the superconducting ground state is calculated in the following approximation [50,51],

see equation (2) above.

The first term arises from scattering between quasiparticle levels above the superconducting ground state, the second term corresponds with the creation of pairs of quasiparticles (neutron energy loss scattering) whilst the final term corresponds with pair condensation (neutron energy gain scattering). At low temperatures the quasiparticle density is small (witness the small specific heat [8]) and the leading contribution is expected to come from the second term where the incident neutron beam stimulates the creation of quasiparticle excitations. A spin singlet (even parity) superconducting ground state is assumed [6,45–48]. The notation is standard: $\xi(\mathbf{k}) = \varepsilon(\mathbf{k}) - \varepsilon_F$ is the normal state single particle energy relative to the normal state Fermi energy, $\Delta(\mathbf{k})$ the gap and $E(\mathbf{k}) = \sqrt{\xi(\mathbf{k})^2 + |\Delta(\mathbf{k})|^2}$ the quasiparticle excitation energy above the superconducting state. The factor $\Phi(\mathbf{q})$ is the phase difference between $\Delta(\mathbf{k})$ and $\Delta(\mathbf{k}+\mathbf{q})$.

Focusing on the second term in equation (2) the key points of the numerical calculations are first illustrated with a semi-quantitative analysis. First we note that at low temperatures the Pauli principle restricts attention to quasiparticle states lying close to the original Fermi surface, $(1 - f(\mathbf{k}+\mathbf{q}) - f(\mathbf{k})) \approx 1$. Turning to the coherence factor, for minimum excitation energy where the quasiparticles have $\xi(\mathbf{k})$, $\xi(\mathbf{k}+\mathbf{q}) = 0$ this reduces to $1 - \cos[\Phi(\mathbf{q})]$ and thus, for a finite response, $\Delta(\mathbf{k}+\mathbf{q})$ must be the negative of $\Delta(\mathbf{k})$ at least over a sizable portion of the zone. The observation of enhanced scattering in the superconducting phase around the antiferromagnetic reciprocal lattice vectors (*i.e.* $\mathbf{q} = \mathbf{Q}_0$ in Eq. (2)) is therefore compatible with an order parameter displaying sign inversion on translation by $\mathbf{Q}_0$ over a significant part of the zone, that is, the observed scattering suggests an *antiferromagnetic* form of Δ be taken, $\Delta(\mathbf{k}) = -\Delta(\mathbf{k}+\mathbf{Q}_0)$ [18–21]. The phase symmetry, zeros either at $\pm\pi/2c$ or at 0 along c^*, is determined by further arguments given below.

Independent of this phase symmetry, the neutron scattering response at $\mathbf{Q}_0$, within the restriction that we consider only states having $\xi(\mathbf{k}) = 0$, is then given by the imaginary part of the Pauli restricted summation $\tilde{\sum}_k 1/(\omega - 2|\Delta_k| + \mathrm{i}\Gamma)$. This is a sum of Lorentzians centred at $2|\Delta_k|$ and of width Γ. In the case that $\Delta(\mathbf{k}) = -\Delta(\mathbf{k}+\mathbf{Q}_0)$ with $|\Delta_k|$ independent of k, the "antiferromagnetic-s-wave" (afm-s-wave) state, the response simplifies to a single Lorentzian centered at 2Δ of damping Γ related to the effective quasiparticle lifetime.

For the union of the low and high frequency modes, equation (1), we use a Lorentzian approximation to represent the low frequency dynamics together with a coupling constant and damped spin wave of the form determined in the normal state. This approach enables a crude self consistency; the full χ_1 which enters the mean field coupling equation (1) is assumed to have the same form as the bare spin susceptibility calculated after equation (2) but with renormalised parameters. The analysis (at $\mathbf{Q}_0$) then yields experimental values for $\Delta(\mathbf{Q}_0)$. Having obtained the magnitude of Δ we compute the anisotropy of the response taking into account the nature of the Fermi surface within two models for $\Delta(\mathbf{q})$.

2.5 Model 1, antiferromagnetic-s-wave

The most primitive approximation for Δ is to keep it constant in magnitude changing sign at $\mathbf{q} = (0,0,\pm\pi/2c)$ or $\mathbf{q} = (0,0,0)$. From the form of the low energy scattering in the superconducting state for small q around $\mathbf{Q}_0$ (Fig. 2 left hand panel) it is unlikely that either the "cylinder" or the "party hat" contribute a significant amount since they would generate low energy excitations predominately for $\mathbf{q}$ parallel to c^*. The observed scattering does not have this anisotropy. We have examined in some detail the response of the "cigar" and "egg" surfaces. Assigning

[1] The breaking of hexagonal symmetry by the antiferromagnetic moment does not play a large role for these small $\mathbf{q}$ vectors.

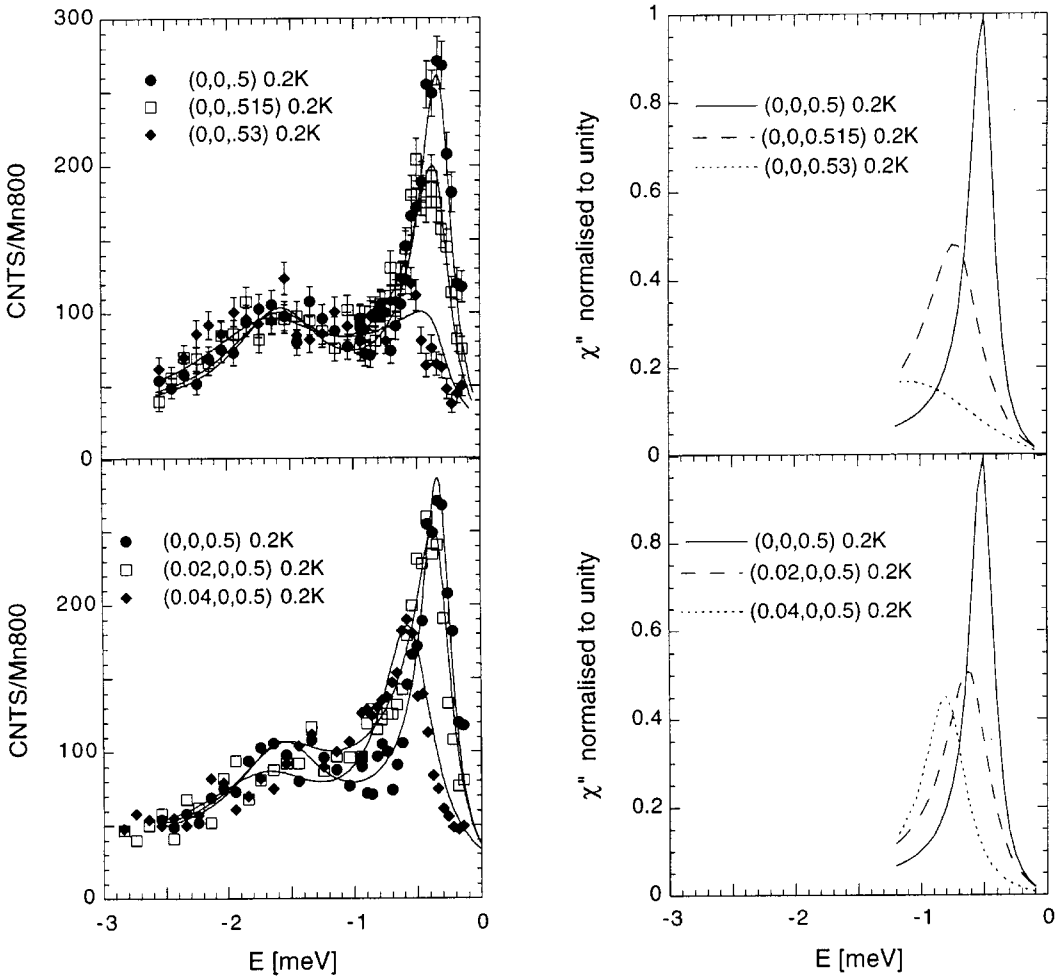

Fig. 2. The low temperature, 0.2 K, scattering around $\mathbf{Q}_0$ is displayed in the left hand frame for $\mathbf{q}$ along c^* and for $\mathbf{q}$ along a^*. The data are fitted with the model susceptibility function discussed in the text (Eq. (1)) taking the experimental resolution into account and with spin wave parameters and coupling constant keeping their values determined above T_c. The model form of χ_1, based on the Lorentzian approximation, is plotted in the right hand frame (top and bottom). The calculations have been normalised to unity at their maximum value which occurs for $\mathbf{Q} = \mathbf{Q}_0$. As in Figure 1 the elastic scattering is not shown.

a sine wave like symmetry to Δ, *i.e.* zero at the Brillouin zone centre would yield no nodes on either the "cigar" or "egg" part of the Fermi surface, conversely, the cosine (A_{1g}) symmetry gives equatorial nodes around the "cigar" shaped sheets located at $\mathbf{q} = (0, 0, \pm\pi/2c)$. In view of the symmetry properties of Δ determined from analyses of tunneling data [22–24], nuclear resonance [40,46,47] and upper critical field measurements [45] we use this latter form [52].

The sum in equation (2) involves the whole f-electron Fermi surface. As in the case of the spin wave response we use the anisotropy of the scattering to identify the principal sheets. To start the calculation we compute (Fig. 3) the form and relative magnitude of response from the "egg" and "cigar" Fermi surface sheets for small q around $\mathbf{Q}_0$ using the second term of equation (2). The curves in Figure 3 are based on parameters extracted from band structure calculations and dHvA data and on the values of $|\Delta|$ and quasiparticle damping rate Γ measured by tunneling [24]. The most poorly known parameter is m^*. A value of $\varepsilon_{\text{Fermi}} = 35$ K has been taken which gives m^* in the range $\sim$ 10$\sim$100 for the "cigar" and "egg" Fermi sheets with average values estimated as 40 and 65 respectively. In the left hand panel of Figure 3 the calculated response from the "egg" sheet of the Fermi surface has been plotted, the curves have been normalised to unity at the maximum of the (0,0,0.5). In the right hand panel of Figure 3 the response from the "cigar" sheet of the Fermi surface is given under the same normalisation. In either case, at $\mathbf{Q}_0$ and the lowest temperatures, the susceptibility which is dominated by the second term in equation (2), has the approximate form of a Lorentzian centered around twice the maximum single particle gap, with the width being determined by the forms of $\varepsilon(\mathbf{k})$ and $\Delta(\mathbf{k})$.

The Lorentzian approximation, with the experimental resolution, the phenomenological spin wave response and the mean field coupling constant determined just above T_c, permits calculation of the solid curves in Figure 2, left hand frame. The values of χ_1'' used in the fits, normalised to unity at $\mathbf{Q}_0$, are given in the right hand frame

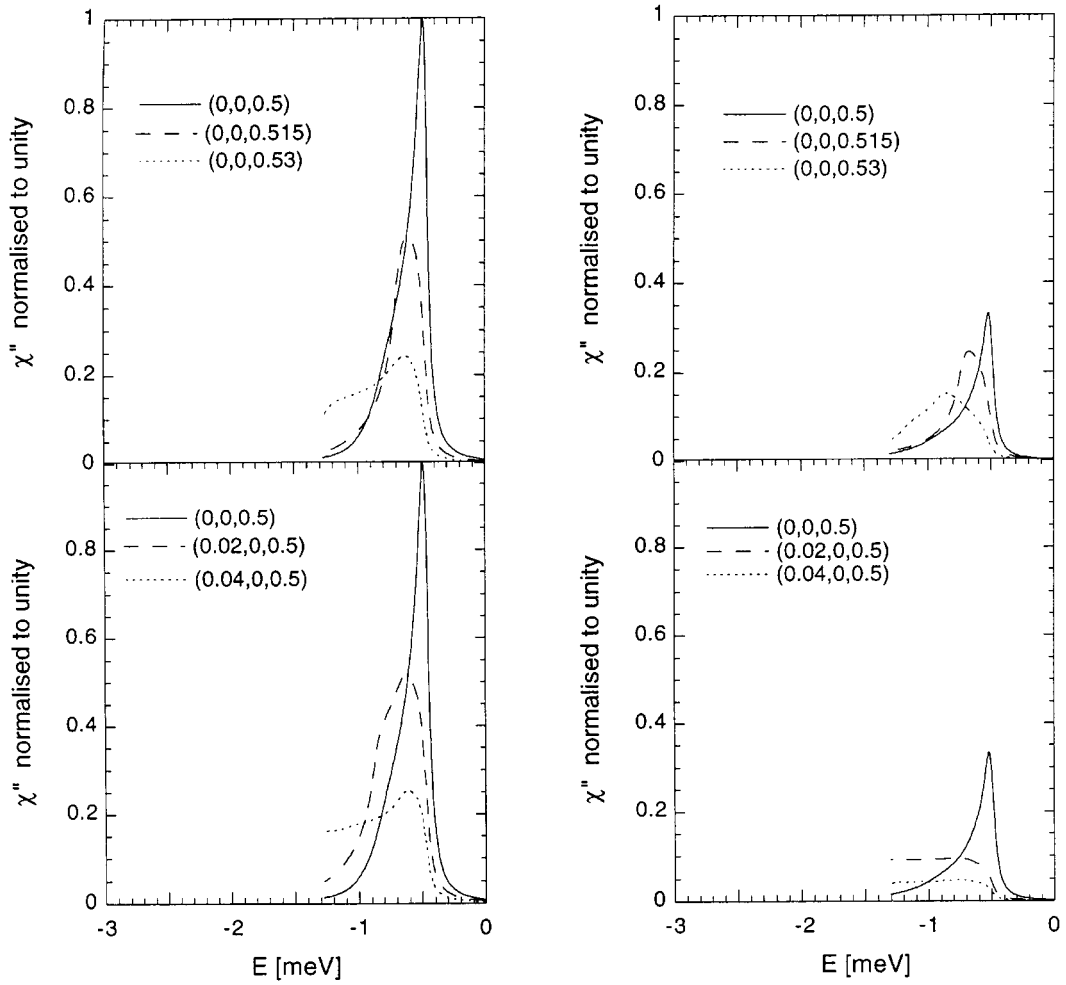

Fig. 3. Calculations based on the second term of equation (2) in the text using the afm-s-wave model for Δ. Parameter values for the Fermi surface are extracted from band structure calculations and dHvA data; the values of Δ and quasiparticle damping rate Γ are those measured by tunneling [24]. The left hand frame gives the response normalised to unity at $\mathbf{Q} = \mathbf{Q}_0$ derived from the "egg" sheet of the Fermi surface. The right hand frame gives the response derived from the "cigar" sheet of the Fermi surface. The response is less isotropic than that in the left hand frame and is approximately three times weaker (see also Fig. 5).

of Figure 2. To complete the consistency loop we now refer back to Figure 3. Two points are clear: first, for the given parameters, the scattering amplitude from the "egg" sheet is approximately three times that calculated from the "cigar", and, as $\mathbf{q}$ increases from $\mathbf{Q}_0$, the response from this sheet has an anisotropy most similar to the experimental data. Second, the Lorentzian form, whilst moderately successful in capturing the calculated lineshape around $\mathbf{Q}_0$ becomes an increasingly poor approximation as one moves out in the zone. As we shall see, Section 2.6, replacing the (unphysical) discontinuous jump in Δ at the zone boundary by a smooth fall off renders the profile more nearly Lorentzian in form by increasing the density of low energy excitations.

2.6 Second model for Δ

Model 1 for $\Delta(k)$ is overly simple. In general nodes at $(0, 0, \pm\pi/2c)$ with A_{1g} symmetry may be built from functions of the form $\Delta(\mathbf{k}) = \sum a_n \cos((2n+1)ck_z)$. Moving away from the "square wave" form of Δ will give a gap of varying magnitude over both the "egg" and "cigar" Fermi surface sheets. We consider how this affects the interpretation of experimental data.

In Figure 4, a model of Δ is given (left hand ordinate) together with the schematic cross-sections of the "egg" and "cigar" Fermi sheets situated in the antiferromagnetic Brillouin zone (right hand ordinate). The increased region of momentum space over which the gap has below maximum value swells the density of low energy excitations out of which to build the dynamic susceptibility in comparison with model 1. This shows up as a tail in the neutron response below the peak at $2\Delta_{\max}$ (Fig. 5) left hand panel for the "egg" and right hand panel for the "cigar", respectively. In particular, around $\mathbf{Q}_0$, the calculated response from the "egg" develops a low energy shoulder due to the almost flat part of the surface which lies close to $(0, 0, \pm\pi/2c)$. The relative intensities of the "egg" and "cigar" contributions remain approximately in the ratio 3:1 as in model 1 and the softening of the square

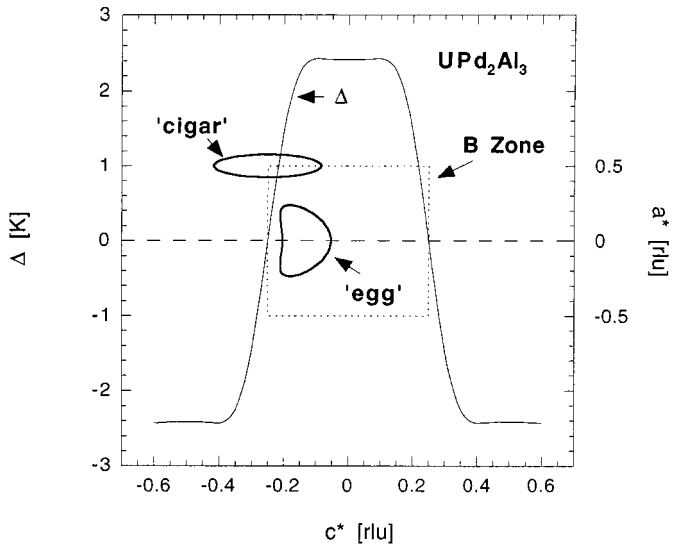

Fig. 4. The plot gives the superposition, on a common c^* abscissa, of the "cosine" energy gap function (left hand ordinate) and the "egg" and "cigar" sheets of the Fermi surface (right hand ordinate). The dotted line marks the zone boundaries along a^* and c^*. The "cosine" profile, model 2, is of the form: $\Delta(q) \propto \cos(q_z c) - \cos(3q_z c)/5 + \cos(5q_z c)/30$.

wave profile for Δ leaves the anisotropy of the calculated response in qualitative agreement with the experimental data.

3 Discussion

3.1 Overview

Experimental reports which strongly favour a spin singlet superconducting state with line nodes about the c^* axis include: nuclear resonance data [40,46,47], the measured μSR reduction in spin susceptibility [6], the angular dependence of the upper critical field [45] and tunneling data [22–24]. The interpretation of the low temperature thermal conductivity [48,49] indicates the need for a node structure yielding quasiparticle excitations with momenta along both c^* and a^* directions. Assuming an ellipsoidal Fermi surface centered at $\mathbf{q} = (0, 0, 0)$ this requires either (i) equatorial and polar nodes or, (ii), nodes lying between the equatorial and polar positions, as for example in the $Y_{2,0}$ state. Alternatively, the data may be compatible with the given, antiferromagnetic, gap structure taken together with those sheets of the Fermi surface which cross the Brillouin zone boundary. Taking into account the Fermi surface topology the proposed form of $\Delta(k)$ is consistent with the requirements of all these experiments.

It has been argued [53], that, if the dominant coupling in the superconducting state involves a given set of (uranium) ions then, the symmetry adapted wave functions appropriate to the group representations of the (hexagonal) lattice may give insight into the permitted symmetries of the order parameter. Reversing the argument, and assuming the pairing wave function to have the symmetry of Δ, the neutron scattering data lend weight to the idea that the coupling may involve neighbouring sheets of U ions on a given magnetic sub-lattice. Such an order parameter might act to lower the on site repulsive part of the interaction and thereby reduce the importance of retardation effects in the pairing. Since we are only interested in quasiparticle excitation energies in the vicinity of Δ strong coupling effects have not been incorporated in the calculation of the neutron scattering cross-section; the gap is taken to be independent of quasiparticle energy and has no imaginary part.

3.2 Tunneling

Tunneling spectra involve two principal data sets by the same group [22–24]. Experiments were performed on films of UPd_2Al_3 first with a relatively thin insulating layer between the sample and the counter electrode [22,23] and later with a more substantial oxide layer [24]. Under the latter conditions, in the given experimental geometry, the tunneling current is highly directional along the crystalline six-fold axis. The surface explored is the "egg". The analysis given in [24] assumes a constant value of Δ over the tunneling states together with a leakage conductivity fixed to model the offset in conductance at the origin. This would be consistent with an afm-s-wave model for Δ. The modified, sum of cosines, form of Δ gives tunneling spectra as the superposition of that arising from two values of the energy gap assuming no interference term. The minimum gap arises from the (almost) flat part of the surface near $(0, 0, \pm\pi/2c)$ and the maximal value from the "apex" situated near (0,0,0). Simulations of tunneling spectra using the Dynes formula [54], reproduced in Figure 6 for the parameters used by Jourdan *et al.* [24] and also for a gap which varies in accordance with model 2, indicate that the experimental data would also be consistent with the latter form of Δ. In addition to the experimental identification of the quasiparticle gap on the "egg" Fermi surface sheet, the tunneling data bring rather direct evidence of a strong interaction between the quasiparticle charge and magnetisation density degrees of freedom on this sheet of the Fermi surface. In the superconducting phase the tunneling spectra exhibit a pronounced oscillation at 1.2 meV, it is proposed that this corresponds with the spin wave gap [24]. Interestingly, it is precisely with the "egg" surface that we identify the anisotropy of the spin wave response around $\mathbf{Q}_0$ yielding a high density of spin wave modes for fluctuations in the a^*-b^* plane.

Tunneling spectra taken with a thinner insulating layer [22,23] give sensitivity to Fermi surface states lying on a cone of greater semi-angle about the c^* axis. In these experiments a clear change of the conductance profile occurs for temperatures greater than 1.2 K indicative of a gap nodal structure. In the light of model 2, as the temperature increases the surface of the "egg" close to $(0, 0, \pm\pi/2c)$ may develop a substantial density of quasiparticle excitations, starting around its lip. This would naturally account for the apparent change in gap symmetry with temperature. Given an approximately BCS form for the temperature dependence of the gap function

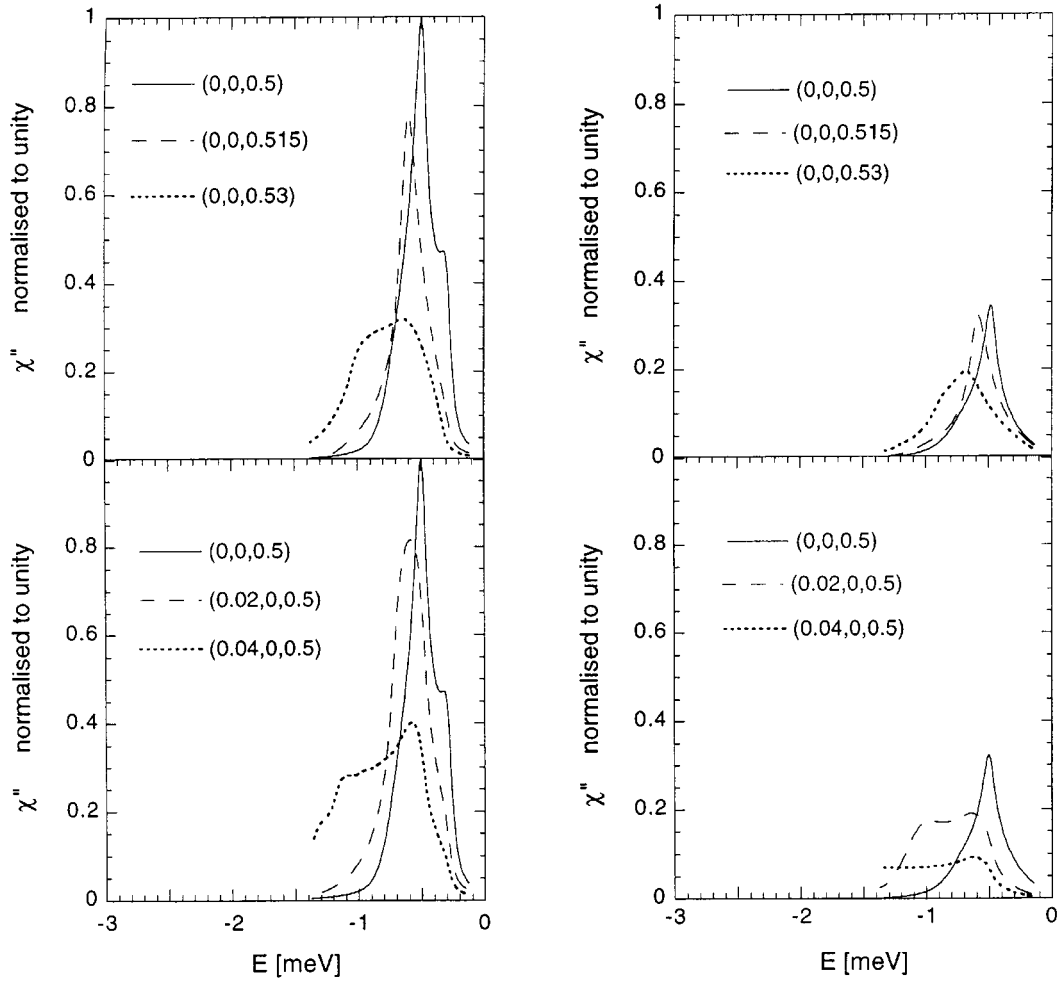

Fig. 5. As in Figure 3 but for model 2 for Δ. The left hand frame gives the response normalised to unity at $\mathbf{Q} = \mathbf{Q}_0$ derived from the "egg" sheet of the Fermi surface. The right hand frame gives the response derived from the "cigar" sheet of the Fermi surface. The response shows an increased low energy spectral weight arising from the "cosine" energy gap profile.

[20,24] one may estimate the onset temperature of significant thermal excitation as $\sim 0.5\Delta$. On the lip of the "egg" near $(0, 0, \pm\pi/2c)$ the gap is estimated ~ 2 K (see Fig. 4) giving an onset temperature around 1 K in accord with the experiment.

3.3 Neutron data, temperature dependence

In the light of this model for the thermal excitation of quasiparticles we examine the temperature dependence of the neutron scattering data at $\mathbf{Q}_0$. The neutron data (Fig. 7) are remarkable in that the observed scattering does not change in magnitude or form until 1.2 K where upon the intensity both falls and starts to develop a strong quasielastic component. The suggested model accounts, at the qualitative level, for these unusual observations: below 1 K the scattering from the nodeless "egg" sheet is essentially temperature independent since $\Delta \gg k_{\mathrm{B}}T$; above 1 K the approximately flat part of the sheet near $(0, 0, \pm\pi/2c)$ yields a Fermi surface area over which thermal activation creates quasiparticle excitations at a rapidly expanding rate. This swells the quasiparticle contribution to the dynamical susceptibility at the cost of the condensate response giving rise to the observed change in spectral form.

4 Conclusion

It has been demonstrated that an analysis of low energy neutron spectra taken below T_{c} is consistent with the notion that one is observing scattering from the condensate. This being so, the symmetry of the gap function is constrained such that $\Delta(\mathbf{k}) = -\Delta(\mathbf{k} + \mathbf{Q}_0)$. Using Fermi surface parameters from the calculated band structure and dHvA data together with quasiparticle gap and lifetimes estimated from tunneling experiments, the measured neutron spectra, at low energies in the superconducting state, appear to be dominated by the scattering anticipated from the "egg" sheets of the Fermi surface. Further, the anisotropy of the scattering for small q near $\mathbf{Q}_0$ also suggests that the "egg" sheet of the Fermi surface is involved in a principal manner in the superconducting state. These conclusions have been reinforced by analysis of other experimental results, notably those obtained from high quality tunneling data [22–24].

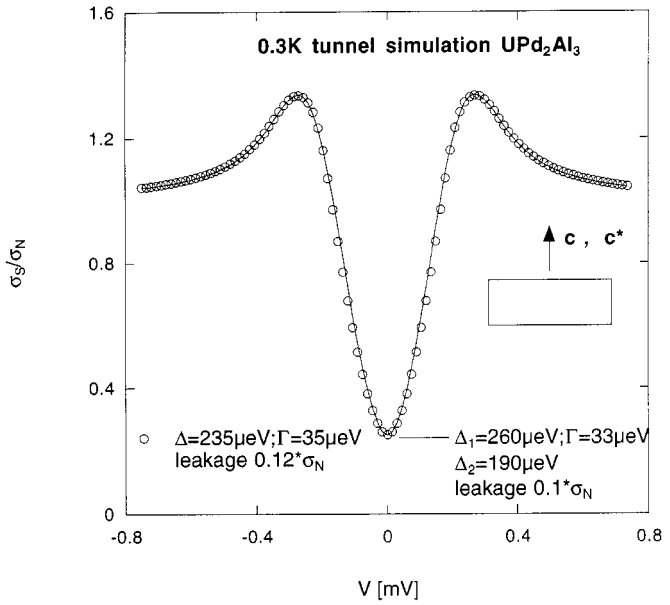

Fig. 6. A simulation of tunneling spectra at 0.3 K using the Dynes formula. Circles are calculated using the parameters derived in [24] whilst the solid line is calculated using the "cosine" form of Δ. Either form appears capable of giving an acceptable interpretation of the experimental data taken for tunneling currents parallel to the crystalline c axis.

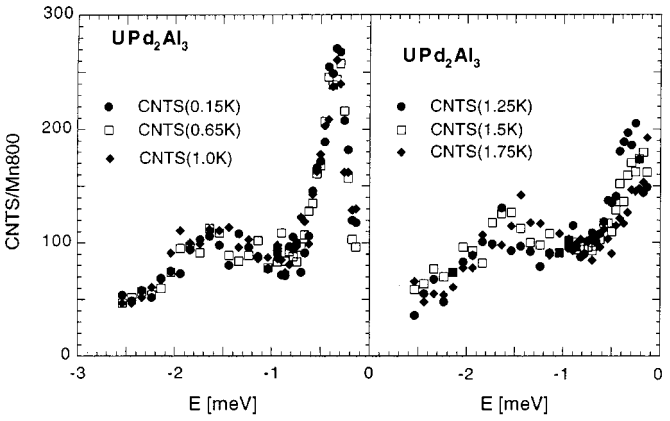

Fig. 7. Neutron scattering intensity at $\mathbf{Q}_0$ as a function of energy transfer for various temperatures below T_c. For temperatures up to 1 K there is negligible change in profile. The rapid change at 1.25 K and above supports the premise that part of the Fermi surface responsible for the scattering should have a reduced energy gap. As in Figure 1 the elastic scattering is not shown.

Other techniques, thermal conductivity and nuclear magnetic resonance, for example, may yield complementary information. On account of the gap, at the lowest temperatures the "egg" sheet will contribute nothing to the heat flux nor to $\omega_{\rm nmr}$ ($\sim$ zero frequency) magnetic excitations; conversely the "cigar", "cylinder" and "party hat" are all able, in principle, to contribute. At low temperatures these experiments then yield complementary information; at higher temperatures, but still below T_c, the thermal excitations on the "egg" sheet may play a significant role. Interestingly, both the upper critical field B_{c2} and the heat capacity exhibit an anomalous temperature dependence. The pronounced changes in the angular dependence of B_{c2} as a function of temperature [45], which are indicative of a cross over from an "s-wave" like gap to a "d-wave" like gap on passing from 0.5 K to 1.5 K, may be qualitatively understood with the suggested model for the thermal evolution of quasiparticle excitations on the lip of the "egg" close to the $\pm\pi/2c$ planes. The heat capacity below T_c exhibits a residual linear term and a strong T^3 term. In addition to an origin of the T^3 term in single quasiparticle excitations, in the presence of strong *magnetic* correlations one may have to consider the role of low energy magnetic fluctuations. The coefficient, ~ 140 mJmol^{-1}K^{-4} [7,8], of the T^3 term in the heat capacity corresponds to a mode of dispersion ~ 5 meV Å. At T_c this implies a range in q of excitation of ~ 0.035 Å^{-1} which lies within the known length scale of magnetic correlations [14–21]. Currently the energy of such a mode lies below our neutron scattering resolution.

It is hoped that this work may stimulate the numerical calculation of several quantities; notably the simulation of altering the electron concentration. For example, the effect of reducing the lattice parameter, mimicking the application of hydrostatic or uniaxial strain, on the shape and position with respect to the antiferromagnetic Brillouin zone boundary of the "egg" Fermi surface. Also it will be of interest to investigate the chemical dependence of critical areas of the Fermi surface on electron concentration at equilibrium lattice parameter. In the former case one might try to unravel the relatively low sensitivity of T_c to pressure [55], in the latter, for example, the role of the substitution of Ni for Pd or the substitution of Ga for Al. Eventually the calculation of the Fermi surfaces in UNi_2Al_3 where the incommensurate magnetic ordering may be linked to the Fermi surface topology and in UPd_2Ga_3 where the double unit cell appears to break a symmetry requirement and no superconductivity has been observed to the lowest temperatures explored [56]. On the theoretical side a more complete picture of the magnetic excitation spectra in antiferromagnetic-superconductors is being sought. Experimentally, the study of greater regions of reciprocal space with high resolution neutron scattering above and below T_c are in progress with the aim to identify further contributions of the f-electron Fermi surface active in the superconducting state. The response at large q away from $\mathbf{Q}_0$ may be expected to give information on possible coupling between Fermi surface sheets. Improved samples, with longer quasiparticle lifetimes are anticipated to yield sharper spectral features improving our understanding of the superconducting state. In parallel, inelastic neutron scattering studies on the UNi_2Al_3 compound have been initiated [57] and the possible use of such a model approach to interpret neutron experiments in other heavy fermion and HiT_c materials is in progress.

The essential input from my experimental colleagues, B. Roessli, N. Sato, N. Aso, A. Hiess, G.H. Lander, Y. Endoh and T. Komatsubara, is gratefully acknowledged. Thanks are due to M. Huth and M. Jourdan for advice on the tunneling

spectra [22–24]; L. Sandratskii and K. Knopfle for endless pictures of the Fermi surface [41]; I. Fomin, J.P. Brison and J. Flouquet for their critical reading of the manuscript.

References

1. J.F. Annett, Adv. Phys. **39**, 83 (1990).
2. J.R. Schrieffer, *Theory of superconductivity* (Benjamin Cummings, London, 1964).
3. C. Geibel, C. Schank, S. Thies, H. Kitazawa, C.D. Bredl, A. Bohm, M. Rau, A. Grauel, R. Caspary, R. Helfrich, U. Ahlheim, G. Weber, F. Steglich, Z. Phys. B **84**, 1 (1991).
4. A. Amato, R. Feyerherm, F.N. Gygax, A. Schenk, M. Weber, R. Caspary, P. Hellmann, C. Schank, C. Geibel, F. Steglich, D.E. MacLaughlin, Knetsch, R.H. Heffner, Europhys. Lett. **19**, 127 (1992).
5. R. Caspary, P. Hellmann, M. Keller, G. Sparn, C. Wassilew, R. Kohler, C. Geibel, C. Schrank, F. Steglich, Phys. Rev. Lett. **71**, 2146 (1993).
6. R. Feyerherm, A. Amato, F.N. Gygax, A. Schenck, C. Geibel, F. Steglich, N. Sato, T. Komatsubara, Phys. Rev. Lett. **73**, 1849 (1994).
7. T. Sakon, K. Imamura, N. Koga, N. Sato, T. Komatsubara, Physica B **199-200**, 154 (1994).
8. F. Steglich, P. Gegenwart, C. Geibel, R. Helfrich, P. Hellmann, M. Lang, A. Link, R. Modler, G. Sparn, N. Buttgen, A. Loidl, Physica B **223**, 1 (1996).
9. A. Krimmel, P. Fisher, B. Roessli, H. Maletta, C. Geibel, C. Schank, A. Grauel, A. Loidl, F. Steglich, Z. Phys. B **86**, 161 (1992).
10. H. Kita, A. Donni, Y. Endoh, K. Kakurai, N. Sato, T. Komatsubara, J. Phys. Soc. Jap. **63**, 726 (1994).
11. L. Paolasini, J.A. Paixao, G.H. Lander, P. Burlet, N. Sato, T. Komatsubara, Phys. Rev. B **49**, 7072 (1994).
12. A. Krimmel, A. Loidl, P. Fisher, B. Roessli, A. Donni, H. Kita, N. Sato, Y. Endoh, T. Komatsubara, C. Geibel, F. Steglich, Solid State Commun. **87**, 829 (1993).
13. B.D. Gaulin, E.D. Isaacs, J.G. Lussier, J.N. Reimers, D. Gibbs, Pzschack, A. Schroder, L. Taillefer, J.D. Garrett, Phys. Rev. Lett. **73**, 890 (1994).
14. N. Sato, N. Aso, G.H. Lander, B. Roessli, T. Komatsubara, Y. Endoh, J. Phys. Soc. Jap. **66**, 1884 (1997).
15. N. Metoki, Y. Haga, Y. Koike, N. Aso, Y. Onuki, J. Phys. Soc. Jap. **66**, 2560 (1997).
16. N. Metoki, Y. Haga, Y. Koike, N. Aso, Y. Onuki, J. Magn. Magn. Mat. **177-181**, 449 (1998).
17. N. Metoki, Y. Haga, Y. Koike, Y. Onuki, Phys. Rev. Lett. **80**, 5417 (1998).
18. N. Bernhoeft, B. Roessli, N. Sato, N. Aso, A. Hiess, G.H. Lander, Y. Endoh, T. Komatsubara, in *Itinerant Electron Magnetism: Fluctuation Effects*, edited by D. Wagner, W. Brauneck, A. Solontsov (Kluwer, 1998).
19. N. Bernhoeft, N. Sato, B. Roessli, N. Aso, A. Hiess, G.H. Lander, Y. Endoh, T. Komatsubara, Phys. Rev. Lett. **81**, 4244 (1998).
20. N. Bernhoeft, B. Roessli, N. Sato, N. Aso, A. Hiess, G.H. Lander, Y. Endoh, T. Komatsubara, Physica B **259-261**, 614-620 (1999).
21. N. Bernhoeft, to appear in *International Workshop on Electron Correlations and Materials Properties*, edited by A. Gonis, N. Kioussis, M. Ciftan (Plenum, 1999).
22. M. Jourdan, M. Huth, J. Hessert, H. Adrian, Physica B **230-232**, 335 (1997).
23. M. Jourdan, M. Huth, S. Moulould, H. Adrian, J. Magn. Magn. Mat. **177-181**, 431 (1998).
24. M. Jourdan, M. Huth, H. Adrian, Nature **398**, 47 (1999).
25. D. Edwards, J. Magn. Magn. Mat. **15-18**, 262 (1980).
26. D. Edwards, J. Phys. F **12**, 1789 (1982).
27. H. Hasegawa, J. Phys. Soc. Jap. **46**, 1504 (1979).
28. Y. Kuromoto, K. Miyake, J. Phys. Soc. Jap. **59**, 2831 (1990).
29. N. Bernhoeft, G.G. Lonzarich, J. Phys. C **7**, 7325 (1995).
30. C. Pépin, M. Lavagna, Phys. Rev. B **59**, 2591 (1999).
31. W. Baltensperger, S. Strassler, Phys. Kondens. Materie **1**, 20 (1963).
32. J. Keller, J. Magn. Magn. Mat. **28**, 193-198 (1982).
33. G. Zwicknagel, P. Fulde, Z. Phys. B **43**, 23 (1981).
34. M.J. Nass, K. Levin, G.S. Grest, Phys. Rev. Lett. **46**, 614 (1981).
35. G.C. Psaltakis, E.W. Fenton, J. Phys. C **16**, 3913 (1983).
36. E.W. Fenton, G.C. Psaltakis, Solid State Commun. **45**, 5 (1982).
37. K. Machida, K. Nokura, T. Matsubara, Phys. Rev. Lett. **44**, 821 (1980).
38. W. Marshall, S.W. Lovesey, *Theory of Thermal Neutron Scattering* (Oxford University Press, 1971).
39. W.J.L. Buyers, T.M. Holden, in *Handbook of the Physics and Chemisrty of the Actinides*, edited by Freeman, Lander (North Holland, 1985), Vol. 2, p. 239.
40. M. Kyogaku, Y. Kitaoka, K. Asayama, C. Geibel, C. Schank, F. Steglich, J. Phys. Soc. Jap. **62**, 4016 (1993).
41. K. Knopfle, A. Mavromaras, L.M. Sandratskii, J. Kubler, J. Phys. Cond. Matter **8**, 901 (1996).
42. Y. Inada, H. Aono, A. Ishiguro, J. Kimura, N. Sato, A. Sawada, T. Komatsubara, Physica B **199**, 119 (1994).
43. Y. Inada, A. Ishiguro, J. Kimura, N. Sato, A. Sawada, T. Komatsubara, H. Yamagami, Physica B **206-207**, 33 (1995).
44. J.B. Sokoloff, Phys. Rev. **185**, 770-782 (1969).
45. J. Hessert, M. Huth, M. Jourdan, H. Adrian, C.T. Rieck, K. Scharnberg, Physica B **230-232**, 373 (1997).
46. K. Matsuda, Y. Kohori, T. Kohara, Phys. Rev. B **55**, 15223 (1997).
47. K. Matsuda, Y. Kohori, T. Kohara, Physica B **259-261**, 640 (1999).
48. M. Chiao, B. Lussier, B. Ellman, L. Taillefer, Physica B **230-232**, 370 (1997).
49. M. Hiroi, M. Sera, N. Kobayashi, Y. Haga, E. Yamamoto, Y. Onuki, J. Phys. Soc. Jap. **66**, 1595 (1997).
50. J.P. Lu, Phys. Rev. Lett. **68**, 125 (1992).
51. M. Lavagna, G. Stemmann, Phys. Rev. B **49**, 4235 (1994).
52. Possible alternative forms of the gap giving antiferromagnetic symmetry are $\Delta(\mathbf{k}) = \sum a_n \cos((2n+1)ck_z)$ or $\Delta(\mathbf{k}) = \sum a_n \sin((2n+1)ck_z)\mathrm{e}^{\mathrm{i}\phi}$, where φ is the angle in the $k_x - k_y$ plane; in an earlier publication (Ref. [21] this list), before information on the anisotropy of the scattering was experimentally available, a gap of sine wave symmetry has been considered.
53. G. Zwicknagl, Adv. Phys. **41**, 203 (1992).
54. R.C. Dynes, V. Narayanamurti, J.P. Garno, Phys. Rev. Lett. **41**, 1509 (1978).
55. P. Link, D. Jaccard, C. Geibel, C. Wassilew, F. Steglich, J. Phys. Cond. Matter C **7**, 373 (1995).
56. S. Sullow, B. Ludoph, B. Becker, G.J. Nieuwenhuys, A.A. Menovsky, J.A. Mydosh, Phys. Rev. B **56**, 846 (1997).
57. N. Aso, B. Roessli, N. Sato, A. Hiess, G.H. Lander, N. Bernhoeft, Y. Endoh, T. Komatsubara, submitted Phys. Rev. B (1999).